A Unified Statistical Approach for Determining Significant Signals in Location and Scale Space Images of Cerebral Activation

K.J. Worsley, S. Marrett*, P. Neelin*, and A.C. Evans*

September 14, 1995

*Department of Mathematics and Statistics, McGill University, 805 Sherbrooke St. West, Montreal, Québec, Canada H3A 2K6, and *McConnell Brain Imaging Centre, Montreal Neurological Institute, 3801 University St., Montreal, Québec, Canada H3A 2B4*

We present a unified P-value for assessing the significance of peaks in statistical fields searched over regions of any shape or size. We extend this to 4-D scale space searches over smoothing filter width as well as location. The results are usable in a wide range of applications, including PET and fMRI, but are discussed with particular reference to PET images which represent changes in cerebral blood flow (CBF) elicited by a specific cognitive or sensorimotor task.

Key words: PET, fMRI, adaptive filters, Euler characteristic, random fields.

Running title: Unified Statistics for Location and Scale Space

Addresses of corresponding author:
Department of Mathematics and Statistics,
McGill University,
805 Sherbrooke St. West,
Montréal,
Québec,
Canada H3A 2K6.
e-mail: keith@zaphod.math.mcgill.ca
ph: 1-514-398-3842
fax: 1-514-398-3899.

1 Introduction

We present a unified statistical theory for assessing the significance of apparent signal observed in noisy difference images. The results are usable in a wide range of applications, including PET and fMRI, but are discussed with particular reference to PET images which represent changes in cerebral blood flow (CBF) elicited by a specific cognitive or sensorimotor task. Our first result, derived in Worsley (1995), is an estimate of the P-value for local maxima of Gaussian, T, χ^2 and F fields over search regions of any shape or size in any number of dimensions. This unifies the P-values for large search areas in 2-D (Friston *et al.*, 1991), large search regions in 3-D (Worsley *et al.*, 1992), and the usual uncorrected p-value at a single pixel or voxel. This makes it possible to restrict the search to small anatomical regions such as the cingulate gyrus or caudate nucleus, or two dimensional regions such as a slice or the cortical surface, or even single voxels. The results are also generalisable to 4-D searches in time as well as space, which may be useful for fMRI.

Our second result is an extension to searches over smoothing filter width, or scale space. PET images of CBF in an activation study are usually smoothed to a resolution much less than that attainable by the PET camera. In many studies the choice of this smoothing is arbitrarily fixed at a 20mm FWHM, and the resulting statistical field or parametric map is searched for local maxima. Poline and Mazoyer (1994) have proposed a 4-D search over smoothing kernel widths as well as location to find local maxima in 1-D scale space as well as 3-D location space. If the peaks are well separated this allows us to estimate the size of regions of activation as well as their location. We avoid repeating the smoothing and statistical analysis on all scans in an experiment by smoothing just the highest resolution statistical field and then correcting its standard deviation. Only a small number of 'fixels', or filter pixels, are required because the 4-D image is very smooth in the scale direction. The result, derived in Siegmund and Worsley (1995), is a unified P-value for the 4-D local maxima that makes it possible to assess the significance of the regions of activation. The price paid for searching in scale space is a small increase in the critical threshold, but this is offset by the increased sensitivity to detect peaks of all widths.

2 Previous results for large search regions

In many PET activation studies, the researcher wishes to compare the CBF under one condition with that under another, or the response of CBF to a covariate such as stimulus intensity. In either case the problem can be analysed as a multiple regression, in which the test statistic of interest is a T or Z statistic evaluated at each voxel (Friston *et al.*, 1995). These images, often called statistical parametric maps (SPM), are then searched for local maxima that might indicate the presence of significant activation. The main problem is to control false positives, that is, the detection of significant peaks when in fact no activation is present.

If the images are finely sampled, that is the voxel size is small relative to the FWHM of the PET camera, then the image can be approximated by a continuous image or *random field*, in which the voxel values are the values of the random field sampled on a lattice of equally spaced points. Local maxima of the voxels are then closely approximated by local

maxima of the continuous random field. The P-value of these (continous) local maxima has a long history in the statistics literature. Early results for two-dimensional random fields, appearing in 1945, were motivated by studies of waves on the ocean surface. More powerful results for arbitrary numbers of dimensions were derived by Russian probabilists in the 1970's, culminating in the papers and book of Robert Adler (Adler, 1981). The result for a stationary Gaussian random field smoothed by a Gaussian point spread function in two dimensions is

$$\mathrm{P}(\mathrm{Max}\ Z \geq t) \approx \frac{\mathrm{Area}}{\mathrm{FWHM}^2}\ \frac{(4\log_e 2)}{(2\pi)^{\frac{3}{2}}} t e^{-\frac{1}{2}t^2}, \tag{1}$$

where Area is the area of the search region and FWHM is the full width at half maximum of the (Gaussian) point spread function. This result was discovered independently by Friston *et al.* (1991), after correction by a factor of $\pi/4$. The result for three dimensions is

$$\mathrm{P}(\mathrm{Max}\ Z \geq t) \approx \frac{\mathrm{Volume}}{\mathrm{FWHM}^3}\ \frac{(4\log_e 2)^{\frac{3}{2}}}{(2\pi)^2} (t^2-1) e^{-\frac{1}{2}t^2}. \tag{2}$$

where Volume is the volume of the search region (see Figure 1). These results (1), (2) are accurate only for large peak heights and large volumes, and no exact P-value exists.

There has been considerable debate about whether the standard deviation of a CBF subtraction should be estimated by the standard deviation at a voxel, or whether the voxel standard deviations can be pooled over all voxels to give a more stable estimator. The former leads to a T-statistic image with degrees of freedom depending on the number of scans (Frston *et al.*, 1991), whereas the latter leads to a Z-statistic (Worsley *et al.*, 1992). The choice ultimately hinges on a trade-off between specificity and sensitivity. The T-statistic has good specificity but lower sensitivity due to the extra variability of the voxel standard deviation; attempts to alleviate this by pooling standard deviations across conditions may bias the specificity. The Z-statistic has a higher sensitivity due to its stable standard deviation, but its specificity is susceptible to fluctuations in the true voxel standard deviation. For a discussion of this issue, see Worsley *et al.* (1995a).

Early work with the T-statistic image was hampered by the lack of an accurate formula for the P-value of local maxima. Friston *et al.* (1991) suggested converting the T-statistic map to a Z-statistic map by probability integral transforms. Although the resulting map is Gaussian at every voxel, its joint distributional behaviour is different from a Gaussian field and the P-value (2) is too small, especially for low degrees of freedom. This problem was solved in Worsley (1994) which gives an accurate formula for the P-value of T-field local maxima. For three dimensions the result is:

$$\mathrm{P}(\mathrm{Max}\ T \geq t) \approx \frac{\mathrm{Volume}}{\mathrm{FWHM}^3}\ \frac{(4\log_e 2)^{\frac{3}{2}}}{(2\pi)^2} \left(\frac{\nu-1}{\nu}t^2 - 1\right)\left(1+\frac{t^2}{\nu}\right)^{-\frac{1}{2}(\nu-1)}, \tag{3}$$

where ν is the degrees of freedom. This result was reported in the last PET Brain'93 meeting in Akita (Worsley *et al.*, 1993).

3 Search regions of any shape or size

Progress since the Akita meeting has been made on two fronts. The first is the problem of small search regions. The P-value formulas given so far are only accurate for large search regions (see Figure 1). This was overcome by results derived in Worsley (1995) which gives a 'unified' formula for Gaussian fields that combines the previous two and three dimensional results (1) and (2) with analogous zero and one dimensional results to give a P-value that is accurate for search regions of (almost) any shape or size:

$$\begin{aligned} \mathrm{P}(\text{Max Z} \geq t) &\approx \text{Euler characteristic } \frac{1}{(2\pi)^{\frac{1}{2}}} \int_t^\infty e^{-\frac{1}{2}u^2} du \\ &+ \frac{\text{2 Caliper diameter}}{\text{FWHM}} \frac{(4\log_e 2)^{\frac{1}{2}}}{(2\pi)} e^{-\frac{1}{2}t^2} \\ &+ \frac{\text{(1/2) Surface area}}{\text{FWHM}^2} \frac{(4\log_e 2)}{(2\pi)^{\frac{3}{2}}} t e^{-\frac{1}{2}t^2} \\ &+ \frac{\text{Volume}}{\text{FWHM}^3} \frac{(4\log_e 2)^{\frac{3}{2}}}{(2\pi)^2} (t^2-1) e^{-\frac{1}{2}t^2}. \end{aligned} \tag{4}$$

The formula (4) is most accurate when the boundary of the search region is smooth relative to the smoothness of the image; it is too conservative for highly convoluted search regions such as the cortex. Instead we suggest using (4) with the convex hull of highly convoluted search regions, which produces a less conservative and more accurate P-value.

The coefficient of the first term in (4) is the Euler characteristic (EC) of the search region, which is 1 for connected regions with no holes. For a convex search region, the caliper diameter is the average, over all rotations, of the height, length and width of a bounding box placed around the search region. Values of these region size measures for a sphere and for a box are:

		Sphere, radius r	Box, $a \times b \times c$
Euler characteristic,	$V_0 =$	1	1
2 Caliper diamater,	$V_1 =$	$4r$	$a+b+c$
(1/2) Surface area,	$V_2 =$	$2\pi r^2$	$ab+bc+ac$
Volume,	$V_3 =$	$(4/3)\pi r^3$	abc

Note that for a box, twice the caliper diameter is the measure of size frequently used by airlines for luggage. $P = 0.05$ thresholds found by equating (4) to 0.05 and solving for t are plotted against search region size in Figure 1. Note that thresholds for the equal-volume cube and equal-area square are slightly higher than for the sphere and disk, respectively.

For voxel data, such as search regions taken from a voxel atlas, the size measures can be calculated as follows. The voxel size δ must be the same in all dimensions. The voxels inside the search region are treated as points on a lattice, and P is the number of such points, E the number of 'edges' joining adjacent points on the lattice, F the number of 'faces' joining a square of 4 adjacent points, and C the number of 'cubes' joining a cube of 8 adjacent points, all of which are inside the search region (see Figure 2). Then

Euler characteristic,	$V_0 = (P - E + F - C)$
2 Caliper diamater,	$V_1 = (E - 2F + 3C)\delta$
(1/2) Surface area,	$V_2 = (F - 3C)\delta^2$
Volume,	$V_3 = C\delta^3$

Table 1 gives $P = 0.05$ thresholds for some structures selected from a voxel atlas (Evans *et al.*, 1991). Note that the large surface area of the 4mm thick shell covering the outer cortex produces a larger threshold than the frontal lobe, even though the frontal lobe has a larger volume. Further details are given in Worsley *et al.* (1995a).

4 Unified P-value for Z, T, χ^2 and F fields

The result (3) can be generalised to other types of random field, such as a T-field. We define the d-dimnsional *resel count* as

$$R_d = V_d/\text{FWHM}^d, \quad d = 0, \ldots, 3. \tag{5}$$

Then the unified formula is

$$\text{P}(\text{Max} \geq t) \approx \sum_{d=0}^{3} R_d \rho_d(t) \tag{6}$$

where $\rho_d(t)$ is the d-dimensional *EC density*, which depends on the threshold t and the type of random field. Table 4, based on results in Worsley (1994), gives the EC densities for a Gaussian field (which matches the previous formula (4)), a T-field (which generalises the earlier result (3)), a χ^2-field and an F-field. $P = 0.05$ thresholds for a T-field, transformed to a Gaussian scale, are shown in Figure 3. Note that the Gaussian is a good approximation for 40 or more degrees of freedom.

5 Unified P-value for scale space searches

The second theoretical development since the Akita meeting is a formula for the P-value of 4-D local scale space local maxima (Seigmund and Worsley, 1995). We assume that the Gaussian images can be modelled as white noise convolved with a Gaussian filter or point response function and let r =(Min FWHM)/(Max FWHM) be the ratio of the FWHM limits. Then the unified P-value, again accurate for search regions of almost any shape or size, is the same as (6) but with the EC densities given in Table 3. $P = 0.05$ thresholds are given in Figure 4 and compared to the equivalent thresholds for a fixed FWHM search. The price paid for searching in scale space is an increase in threshold of about 0.8 over the threshold for a fixed 20mm FWHM search.

The practical issues of searching scale space are dealt with in some detail in Worsley *et al* (1995b), which shows that: only a small number of filter widths or 'fixels' are needed ($\approx$13), equally spaced on a log scale; only the highest resolution Gaussian image needs to be smoothed, not all the data; the standard deviation can be corrected by using the spatial correlation function. A drawback to the method is that close sharp foci are detected as one

large region. In this case, we suggest that peaks should be inspected for 'bifurcations' in scale space slices.

An example of an application to an experiment in pain perception (Coghill *et al.*, 1994) is shown in Table 4. The data were smoothed from 6.8 to 34mm FWHM ($r = 5$) and searched inside the whole brain search region whose volume measures are given in the last line of Table 1. The formulas (5), (6) and Table 3 were used to calculate P-values for 4-D scale space peaks. Note that the scale space peaks are nearly always larger and more significant than the peaks from a fixed scale search at 20, 20 and 7.4mm FWHM in the x, y and z directions. More importantly, two small foci were discovered in the scale space search that were overlooked in the fixed scale search, presumeably because they were oversmoothed. Figure 5 shows scale space slices through the largest peak, which indicate a bifurcation that suggests that the largest peak is in fact composed of two smaller foci 2cm apart in the y direction. Further details are given in Worsley *et al.* (1995b).

References

Adler R.J. 1981. *The Geometry of Random Fields.* Wiley, New York.

Coghill, R.C., Talbot, J.D., Evans, A.C., Meyer, E., Gjedde, A., Bushnell, M.C., and Duncan, G.H. 1994). Distributed processing of pain and vibration by the human brain. *Journal of Neuroscience* **14**:4095-4108.

Evans, A.C., Marrett, S., Torrescorzo, J., Ku, S., and Collins, L. 1991. MRI-PET correlative analysis using a volume of interest (VOI) atlas. *Journal of Cerebral Blood Flow and Metabolism* **11(2)**:A69-A78.

Friston, K.J., Frith, C.D., Liddle, P.F., and Frackowiak, R.S.J. 1991. Comparing functional (PET) images: the assessment of significant change, *Journal of Cerebral Blood Flow and Metabolism* **11**:690-699.

Friston, K.J., Holmes, A.P., Worsley, K.J., Poline, J-B., Frith, C.D., and Frackowiak, R.S.J. 1995. Statistical parametric maps in functional imaging: A general approach. *Human Brain Mapping*, **2**:189-210.

Poline J.B. and Mazoyer B.M. 1994. Enhanced detection in brain activation maps using a multifiltering approach. *Journal of Cerebral Blood Flow and Metabolism* **14**:639-42.

Siegmund, D.O and Worsley, K.J. 1995. Testing for a signal with unknown location and scale in a stationary Gaussian random field. *Annals of Statistics* **23**:608-639.

Worsley, K.J., Evans, A.C., Marrett, S. and Neelin, P. (1992). A three dimensional statistical analysis for CBF activation studies in human brain. *Journal of Cerebral Blood Flow and Metabolism* **12**: 900-918.

Worsley K.J., Evans, A.C., Marrett, S., and Neelin, P. 1993. Detecting and estimating the regions of activation in CBF activation studies in human brain. *Quantification of Brain Function: Tracer kinetics and image analysis in brain PET, eds. K. Uemura, N. Lassen, T. Jones and I. Kanno* :535-548.

Worsley, K.J. 1994. Local maxima and the expected Euler characteristic of excursion sets of χ^2 F and t fields. *Advances in Applied Probability* **26**:13-42.

Worsley, K.J. 1995. Estimating the number of peaks in a random field using the Hadwiger characteristic of excursion sets, with applications to medical images. *Annals of Statistics* **23**:640-669.

Worsley, K.J., Marrett, S., Neelin, P., Vandal, A.C., Friston, K.J., and Evans, A.C. 1995a. A unified statistical approach for determining significant signals in images of cerebral activation. *Human Brain Mapping*, submitted.

Worsley, K.J., Marrett, S., Neelin, P., and Evans, A.C. 1995b. Searching scale space for activation in PET images. *Human Brain Mapping*, submitted.

TABLE 1. EXAMPLES FROM A VOXEL ATLAS, FWHM=20MM, P=0.05

Search region	V_0	V_1, cm	V_2, cm^2	V_3, cm^3	t
Single voxel	1	0	0	0	1.64
Globus Pallidus	0	8	9	2	2.78
Head of Caudate	0	12	19	5	3.02
Thalamus	1	10	21	9	3.05
Putamen	1	15	27	9	3.15
Cingulate	0	26	39	12	3.27
Occipital Lobe	-1	21	92	57	3.55
Temporal	0	34	147	104	3.71
Parietal	1	30	148	116	3.72
Frontal	1	39	214	189	3.84
4mm shell	2	1	829	127	4.04
Whole brain	1	41	428	1227	4.23

TABLE 2A. GAUSSIAN FIELD

$$\begin{aligned}
\rho_0(t) &= \int_t^\infty \frac{1}{(2\pi)^{\frac{1}{2}}} e^{-\frac{1}{2}u^2} du \\
\rho_1(t) &= \frac{(4\log_e 2)^{\frac{1}{2}}}{2\pi} e^{-\frac{1}{2}t^2} \\
\rho_2(t) &= \frac{(4\log_e 2)}{(2\pi)^{\frac{3}{2}}} t e^{-\frac{1}{2}t^2} \\
\rho_3(t) &= \frac{(4\log_e 2)^{\frac{3}{2}}}{(2\pi)^2} (t^2-1) e^{-\frac{1}{2}t^2}
\end{aligned}$$

TABLE 2B. T-FIELD WITH ν DEGREES OF FREEDOM, $\nu \geq d$

$$\begin{aligned}
\rho_0(t) &= \int_t^\infty \frac{\Gamma\left(\frac{\nu+1}{2}\right)}{(\nu\pi)^{\frac{1}{2}}\Gamma\left(\frac{\nu}{2}\right)} \left(1+\frac{u^2}{\nu}\right)^{-\frac{1}{2}(\nu+1)} du \\
\rho_1(t) &= \frac{(4\log_e 2)^{\frac{1}{2}}}{2\pi} \left(1+\frac{t^2}{\nu}\right)^{-\frac{1}{2}(\nu-1)} \\
\rho_2(t) &= \frac{(4\log_e 2)}{(2\pi)^{\frac{3}{2}}} \frac{\Gamma\left(\frac{\nu+1}{2}\right)}{\left(\frac{\nu}{2}\right)^{\frac{1}{2}}\Gamma\left(\frac{\nu}{2}\right)} t \left(1+\frac{t^2}{\nu}\right)^{-\frac{1}{2}(\nu-1)} \\
\rho_3(t) &= \frac{(4\log_e 2)^{\frac{3}{2}}}{(2\pi)^2} \left(\frac{\nu-1}{\nu}t^2-1\right) \left(1+\frac{t^2}{\nu}\right)^{-\frac{1}{2}(\nu-1)}
\end{aligned}$$

TABLE 2C. χ^2-FIELD WITH ν DEGREES OF FREEDOM

$$\begin{aligned}
\rho_0(t) &= \int_t^\infty \frac{u^{\frac{1}{2}(\nu-2)}e^{-\frac{1}{2}u}}{2^{\frac{\nu}{2}}\Gamma\left(\frac{\nu}{2}\right)}du \\
\rho_1(t) &= \frac{(4\log_e 2)^{\frac{1}{2}}}{(2\pi)^{\frac{1}{2}}}\frac{t^{\frac{1}{2}(\nu-1)}e^{-\frac{1}{2}t}}{2^{\frac{1}{2}(\nu-2)}\Gamma\left(\frac{\nu}{2}\right)} \\
\rho_2(t) &= \frac{(4\log_e 2)}{(2\pi)}\frac{t^{\frac{1}{2}(\nu-2)}e^{-\frac{1}{2}t}}{2^{\frac{1}{2}(\nu-2)}\Gamma\left(\frac{\nu}{2}\right)}[t-(\nu-1)] \\
\rho_3(t) &= \frac{(4\log_e 2)^{\frac{3}{2}}}{(2\pi)^{\frac{3}{2}}}\frac{t^{\frac{1}{2}(\nu-3)}e^{-\frac{1}{2}t}}{2^{\frac{1}{2}(\nu-2)}\Gamma\left(\frac{\nu}{2}\right)}[t^2-(2\nu-1)t+(\nu-1)(\nu-2)]
\end{aligned}$$

TABLE 2D. F-FIELD WITH k AND ν DEGREES OF FREEDOM, $k+\nu > d$

$$\begin{aligned}
\rho_0(t) &= \int_t^\infty \frac{\Gamma\left(\frac{\nu+k-2}{2}\right)}{\Gamma\left(\frac{\nu}{2}\right)\Gamma\left(\frac{k}{2}\right)}\frac{k}{\nu}\left(\frac{ku}{\nu}\right)^{\frac{1}{2}(k-2)}\left(1+\frac{ku}{\nu}\right)^{-\frac{1}{2}(\nu+k)}du \\
\rho_1(t) &= \frac{(4\log_e 2)^{\frac{1}{2}}}{(2\pi)^{\frac{1}{2}}}\frac{\Gamma\left(\frac{\nu+k-1}{2}\right)2^{\frac{1}{2}}}{\Gamma\left(\frac{\nu}{2}\right)\Gamma\left(\frac{k}{2}\right)}\left(\frac{kt}{\nu}\right)^{\frac{1}{2}(k-1)}\left(1+\frac{kt}{\nu}\right)^{-\frac{1}{2}(\nu+k-2)} \\
\rho_2(t) &= \frac{(4\log_e 2)}{2\pi}\frac{\Gamma\left(\frac{\nu+k-2}{2}\right)}{\Gamma\left(\frac{\nu}{2}\right)\Gamma\left(\frac{k}{2}\right)}\left(\frac{kt}{\nu}\right)^{\frac{1}{2}(k-2)}\left(1+\frac{kt}{\nu}\right)^{-\frac{1}{2}(\nu+k-2)} \\
&\times \left[(\nu-1)\frac{kt}{\nu}-(k-1)\right] \\
\rho_3(t) &= \frac{(4\log_e 2)^{\frac{3}{2}}}{(2\pi)^{\frac{3}{2}}}\frac{\Gamma\left(\frac{\nu+k-3}{2}\right)2^{-\frac{1}{2}}}{\Gamma\left(\frac{\nu}{2}\right)\Gamma\left(\frac{k}{2}\right)}\left(\frac{kt}{\nu}\right)^{\frac{1}{2}(k-3)}\left(1+\frac{kt}{\nu}\right)^{-\frac{1}{2}(\nu+k-2)} \\
&\times \left[(\nu-1)(\nu-2)\left(\frac{kt}{\nu}\right)^2-(2\nu k-\nu-k-1)\left(\frac{kt}{\nu}\right)+(k-1)(k-2)\right]
\end{aligned}$$

TABLE 3. SCALE SPACE GAUSSIAN FIELD

$$
\begin{aligned}
\rho_0(t) &= \frac{1}{(2\pi)^{\frac{1}{2}}}\left\{\sqrt{\frac{3}{4\pi}}(-\log_e r)e^{-\frac{1}{2}t^2} + \int_t^\infty e^{-\frac{1}{2}u^2}du\right\} \\
\rho_1(t) &= \frac{(4\log_e 2)^{\frac{1}{2}}}{(2\pi)}\left\{\sqrt{\frac{3}{4\pi}}(1-r)t + \frac{1+r}{2}\right\}e^{-\frac{1}{2}t^2} \\
\rho_2(t) &= \frac{(4\log_e 2)}{(2\pi)^{\frac{3}{2}}}\left\{\sqrt{\frac{3}{4\pi}}\frac{1-r^2}{2}\left(t^2-\frac{1}{3}\right) + \frac{1+r^2}{2}t\right\}e^{-\frac{1}{2}t^2} \\
\rho_3(t) &= \frac{(4\log_e 2)^{\frac{3}{2}}}{(2\pi)^2}\left\{\sqrt{\frac{3}{4\pi}}\frac{1-r^3}{3}(t^3-t) + \frac{1+r^3}{2}(t^2-1)\right\}e^{-\frac{1}{2}t^2}
\end{aligned}
$$

TABLE 4. SIGNIFICANT PEAKS IN COGHILL *et al.* (1994)

	Location (mm) in scale space						Fixed scale	
Peaks	x	y	z	FWHM	Max	P	Max	P
Increases:								
R SII/anterior insula	35	-2	10	22.7	6.56	0.0000	5.65	0.0006
R SMA (Inferior)	4	-2	54	22.7	6.22	0.0001	5.00	0.014
R Thalamus	11	-19	-3	17.4	5.73	0.0012	5.36	0.0025
L Anterior insula	-33	13	7	6.8	4.86	0.0824	3.72	1.96
R SI	24	-28	57	19.9	4.77	0.12	4.02	0.72
L Putamen	-25	5	0	19.9	4.76	0.12	4.57	0.089
R Caudate	-12	-2	15	6.8	4.73	0.14	-	-
Decreases:								
R Posterior cingulate	5	-59	25	15.2	4.86	0.082	5.14	0.0072
M Posterior cingulate	1	-42	30	11.6	4.54	0.31	-	-

Figure 1. Max Z, FWHM=20mm, P=0.05

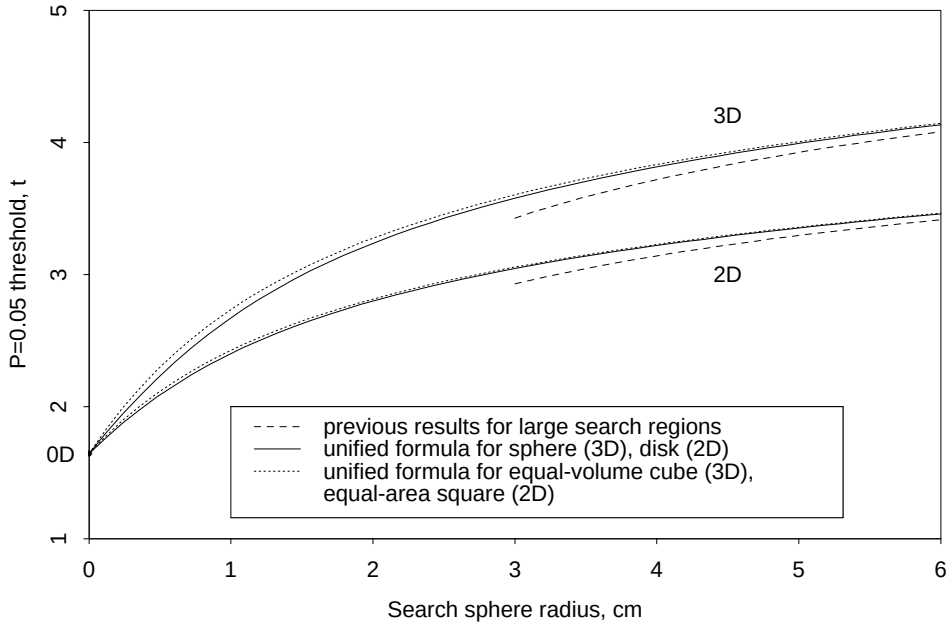

Figure 1:

Figure 2. P=14, E=21, F=9, C=1
V0=1, V1=6, V2=6, V3=1

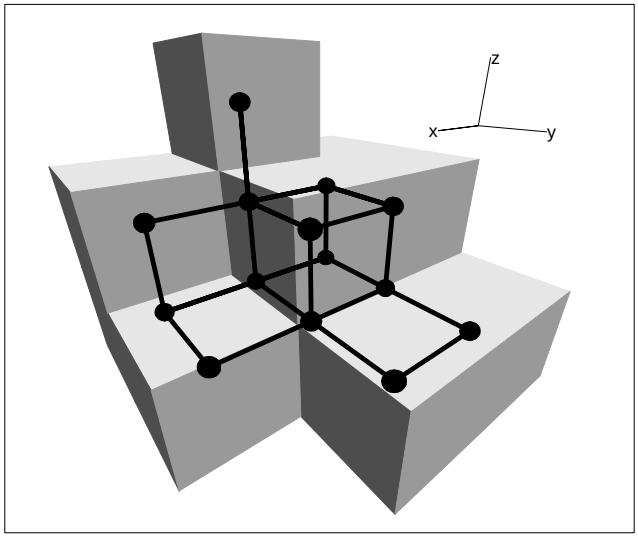

Figure 2:

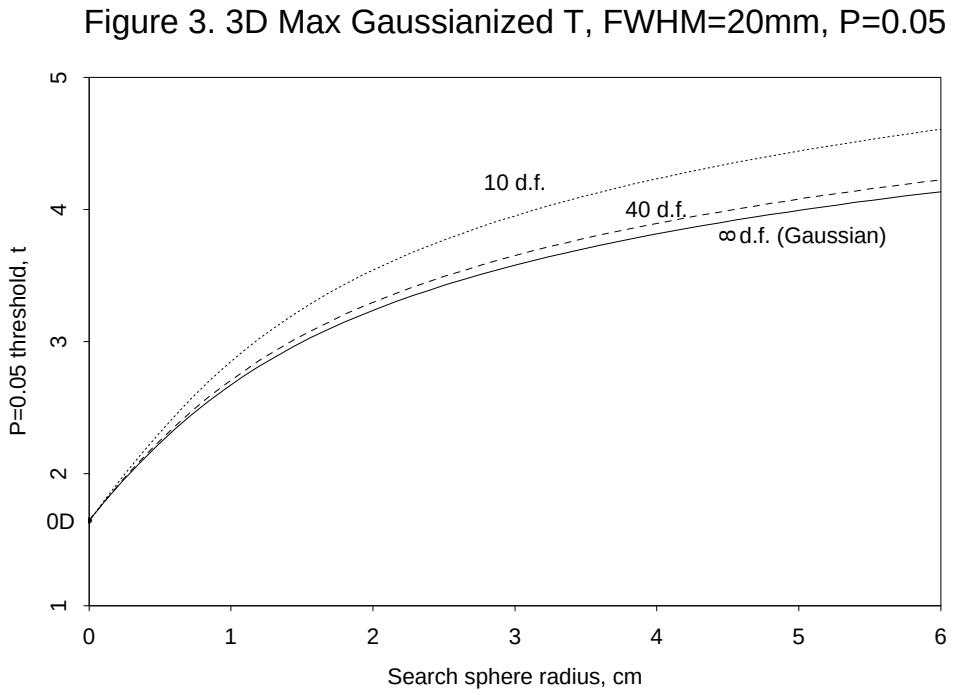
Figure 3. 3D Max Gaussianized T, FWHM=20mm, P=0.05
P=0.05 threshold, t
Search sphere radius, cm
10 d.f.
40 d.f.
∞ d.f. (Gaussian)
0D
1
2
3
4
5
6

Figure 3:

Figure 4. Scale space, P=0.05

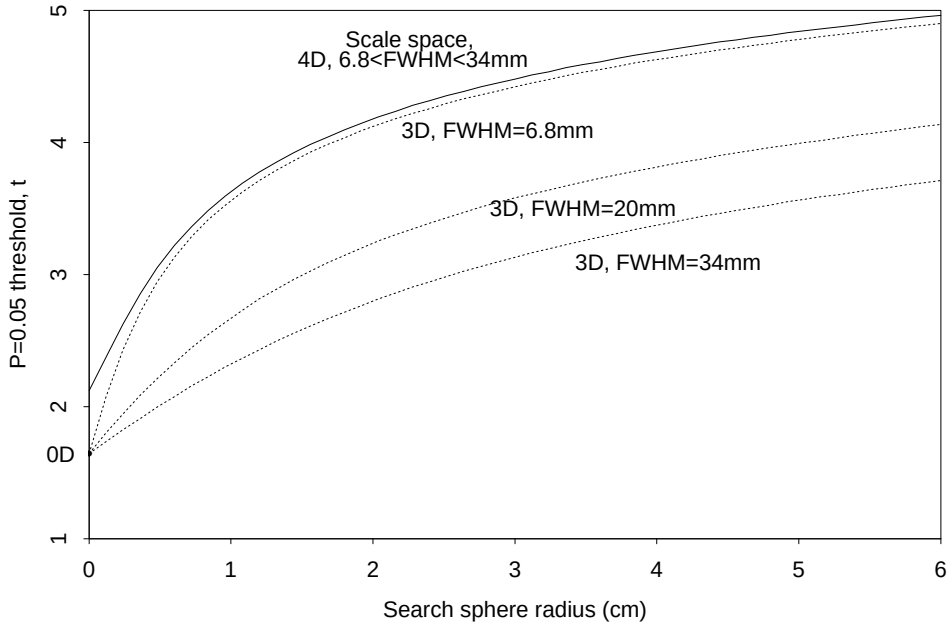

Figure 4:

Figure 5. Scale space slices

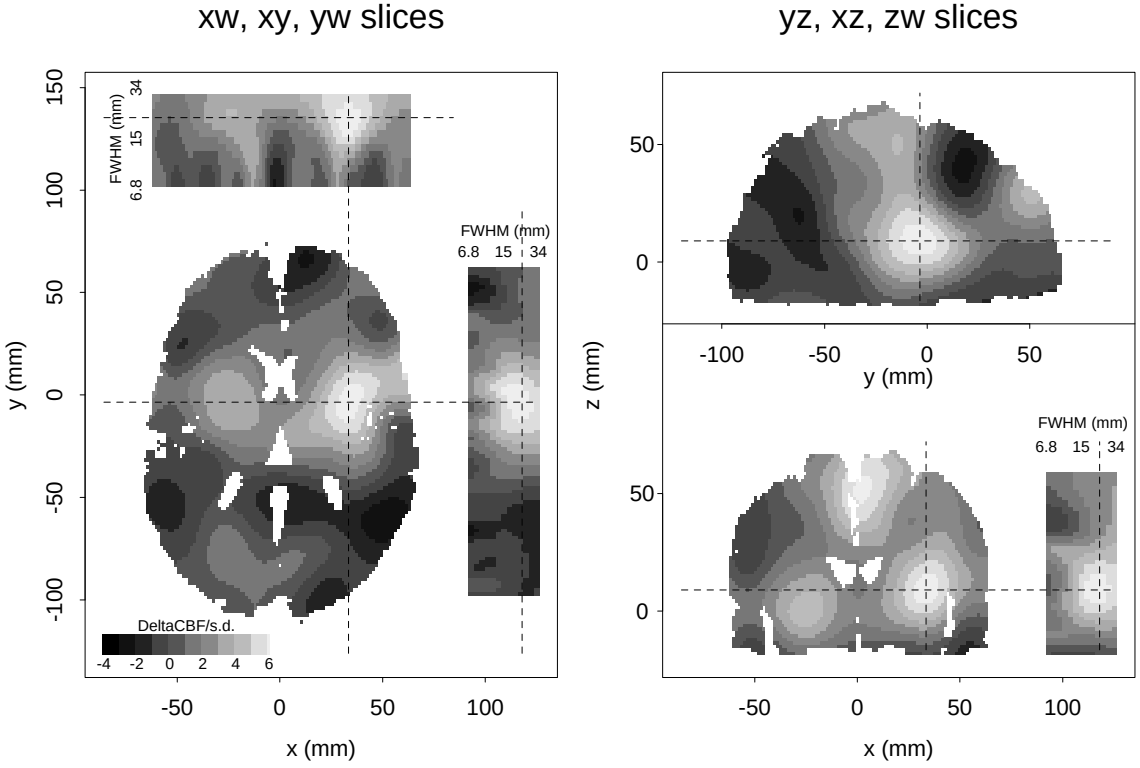

Figure 5: